Dipolar Antiferromagnetism and Quantum Criticality in $LiErF_4$

Conradin Kraemer *et al.*

Science **336**, 1416 (2012);
DOI: 10.1126/science.1221878

as hyperfine interaction mechanism, will probably destroy the conservation of the twisted spin. However, the relevant inelastic lifetime increases as $\sim T^{-1}$ (T, temperature) and eventually becomes on the order of a nanosecond at $T \sim 0.1$ K (*26*, *27*); the BAP mechanism is absent in n-type materials. Additionally, the typical time scale of the spin lifetime resulting from hyperfine coupling is estimated at ~1 ns in n-type GaAs (i.e., longer than 400 ps). The cubic Dresselhaus SOI β_3 of $GaAs/Al_{0.3}Ga_{0.7}As$ quantum well samples is the dominant term causing the relaxation of the PSH, which is regarded as the nonpure gauge potential giving finite $\hat{F}_{\mu\nu}$, and gives the elastic EY and DP mechanisms (*20*). The enhanced spin lifetime on the order of 0.8 ns obtained in (*20*) is already long enough for the purpose of the spin-orbit echo discussed above. Therefore, it is anticipated that the spin-orbit echo can be tested at $T \sim 0.1$ K with the Rashba SOI tuned by electric field with the help of the optical grating method, as in (*20*).

References and Notes

1. S. A. Wolf *et al.*, *Science* **294**, 1488 (2001).
2. R. J. Elliott, *Phys. Rev.* **96**, 266 (1954).
3. Y. Yafet, in *Solid State Physics*, F. Seitz, D. Turnbull, Eds. (Academic, New York, 1963), vol. 14, p. 2.
4. M. I. D'yakonov, V. I. Perel, *Sov. Phys. JETP* **33**, 1053 (1971).
5. M. I. D'yakonov, V. I. Perel, *Sov. Phys. Solid State* **13**, 3023 (1971).
6. G. L. Bir, A. G. Aronov, G. E. Pikus, *Sov. Phys. JETP* (Engl. transl.) **42**, 705 (1975) [transl. from *Zh. E'ksp. Teor. Fiz.* **69**, 1382 (1975)].
7. J. M. Kikkawa, D. D. Awschalom, *Phys. Rev. Lett.* **80**, 4313 (1998).
8. R. I. Dzhioev *et al.*, *Phys. Rev. B* **66**, 245204 (2002).
9. L. H. Thomas, *Nature* **117**, 514 (1926).
10. J. Fröhlich, U. M. Studer, *Rev. Mod. Phys.* **65**, 733 (1993).
11. P.-Q. Jin, Y.-Q. Li, F.-C. Zhang, *J. Phys. Math. Gen.* **39**, 7115 (2006).
12. B. W. A. Leurs, Z. Nazario, D. Santiago, J. Zaanen, *Ann. Phys.* **323**, 907 (2008).
13. T. W. Chen, C. M. Huang, G. Y. Guo, *Phys. Rev. B* **73**, 235309 (2006).
14. Y. Wang, K. Xia, Z. B. Su, Z. Ma, *Phys. Rev. Lett.* **96**, 066601 (2006).
15. R. Shen, Y. Chen, Z. D. Wang, D. Y. Xing, *Phys. Rev. B* **74**, 125313 (2006).
16. D. Culcer *et al.*, *Phys. Rev. Lett.* **93**, 046602 (2004).
17. J. Shi, P. Zhang, D. Xiao, Q. Niu, *Phys. Rev. Lett.* **96**, 076604 (2006).
18. C. N. Yang, R. L. Mills, *Phys. Rev.* **96**, 191 (1954).
19. B. A. Bernevig, J. Orenstein, S.-C. Zhang, *Phys. Rev. Lett.* **97**, 236601 (2006).
20. J. D. Koralek *et al.*, *Nature* **458**, 610 (2009).
21. For details, see the supplementary materials on *Science* Online.
22. N. Sugimoto, N. Nagaosa, http://arxiv.org/abs/1205.6629.
23. S. Murakami, N. Nagaosa, S.-C. Zhang, *Science* **301**, 1348 (2003).
24. J. Sinova *et al.*, *Phys. Rev. Lett.* **92**, 126603 (2004).
25. T. Koga, J. Nitta, T. Akazaki, H. Takayanagi, *Phys. Rev. Lett.* **89**, 046801 (2002).
26. B. J. F. Lin, M. A. Paalanen, A. C. Gossard, D. C. Tsui, *Phys. Rev. B* **29**, 927 (1984).
27. F. E. Meijer, A. Morpurgo, T. Klapwijk, T. Koga, J. Nitta, *Phys. Rev. B* **70**, 201307(R) (2004).

Acknowledgments: We thank K. Richter, V. Krueckl, and S. Onoda for fruitful discussion. This work is supported by Grant-in-Aid for Scientific Research from the Ministry of Education, Culture, Sports, Science and Technology of Japan; Strategic International Cooperative Program (Joint Research Type) from Japan Science and Technology Agency; and the Funding Program for World-Leading Innovative Research and Development on Science and Technology, Japan.

Supplementary Materials

www.sciencemag.org/cgi/content/full/336/6087/1413/DC1
Supplementary Text
Fig. S1
References (*28*–*30*)

1 December 2011; accepted 27 April 2012
10.1126/science.1217346

Dipolar Antiferromagnetism and Quantum Criticality in $LiErF_4$

Conradin Kraemer,[1,2] Neda Nikseresht,[1] Julian O. Piatek,[1] Nikolay Tsyrulin,[1] Bastien Dalla Piazza,[1] Klaus Kiefer,[3] Bastian Klemke,[3] Thomas F. Rosenbaum,[4] Gabriel Aeppli,[5] Ché Gannarelli,[5] Karel Prokes,[3] Andrey Podlesnyak,[6] Thierry Strässle,[2] Lukas Keller,[2] Oksana Zaharko,[2] Karl W. Krämer,[7] Henrik M. Rønnow[1]*

Magnetism has been predicted to occur in systems in which dipolar interactions dominate exchange. We present neutron scattering, specific heat, and magnetic susceptibility data for $LiErF_4$, establishing it as a model dipolar-coupled antiferromagnet with planar spin-anisotropy and a quantum phase transition in applied field $H_{c\|} = 4.0 \pm 0.1$ kilo-oersteds. We discovered non–mean-field critical scaling for the classical phase transition at the antiferromagnetic transition temperature that is consistent with the two-dimensional XY/h_4 universality class; in accord with this, the quantum phase transition at H_c exhibits three-dimensional classical behavior. The effective dimensional reduction may be a consequence of the intrinsic frustrated nature of the dipolar interaction, which strengthens the role of fluctuations.

The dipolar force between magnetic moments—a consequence of Maxwell's fundamental laws for electromagnetism—is present in all magnetic systems, from classical to quantum magnets, from bulk materials to nanoparticles. More than a half century ago, Luttinger and Tisza (*1*) discussed whether a polarized state of matter can be induced by classical dipole-dipole interactions alone and in the absence of short-range forces such as exchange interactions. They conjectured that both ferromagnetic (FM) and antiferromagnetic (AFM) order can arise, depending on the geometrical arrangement of the dipoles. When the modern theory of critical phenomena was developed, dipolar-coupled ferromagnets—in which the dipoles are atomic magnetic moments—presented material realizations on which concepts could be tested. Being three-dimensional (3D) systems, they were at the upper marginal dimension for the applicability of mean-field (MF) theory. This resulted in logarithmic corrections, which could be calculated exactly and agreed with the measured behavior around the classical phase transition (*2*). In the context of quantum phase transitions (QPTs), anisotropic dipolar systems are excellent realizations of, for example, the Ising model in a transverse field. In dipolar systems, the anisotropy ratio for the dipolar interaction scales as the square of the anisotropy ratio for response to an external magnetic field, and as a consequence, even for modest single-ion anisotropy the dipolar interaction along the hard axis is much smaller than along the easy axis. This hierarchy of scales is much harder to achieve in exchange-coupled systems in which the moment-carrying electron wave functions are responsible for both the exchange and single-ion anisotropies.

An excellent testing ground for the physics of dipolar-coupled systems are the lithium rare earth (*RE*) tetrafluorides, $LiREF_4$, in which tightly bound 4*f* electrons are far enough apart for the dipolar interactions to dominate exchange interactions. Another major advantage of the $LiREF_4$ family is the possibility of isostructural dilution with nonmagnetic yttrium, $LiRE_xY_{1-x}F_4$—permitting experiments from isolated dipoles (*3*) through disordered interacting dipoles forming spin glass states (*4*–*6*)—to the undiluted limit $LiREF_4$. To date, activity has centered on the Ising-like ferromagnets $LiTbF_4$ (*2*) and $LiHoF_4$ (*7*) and their respective dilution series (*8*). Here, we focus on an AFM member of the family $LiErF_4$ and address the magnetic order, the classical phase transition, and the transition and fluctuations about the quantum critical point.

Known as *RE*:YLF, very dilute ($x < 1\%$) $LiRE_xY_{1-x}F_4$ is used commercially in laser technology because of the long lifetimes of the crystal field energy levels of isolated RE^{3+} ions. The crystal field also sets the stage for low-temperature collective properties. The electric field from neighboring ions act differently on the orbital wave-

[1]Laboratory for Quantum Magnetism, Ecole Polytechnique Fédérale de Lausanne (EPFL), 1015 Lausanne, Switzerland. [2]Laboratory for Neutron Scattering, Paul Scherrer Institute, 5232 Villigen, Switzerland. [3]Helmholtz-Zentrum Berlin, 14109 Berlin Wannsee, Germany. [4]James Franck Institute and Department of Physics, University of Chicago, Chicago, IL 60637, USA. [5]London Centre for Nanotechnology and Department of Physics and Astronomy, University College London, London WC1E 6BT, UK. [6]Oak Ridge National Laboratory, Spallation Neutron Source, Oak Ridge, TN 37831, USA. [7]Department of Chemistry and Biochemistry, University of Bern, 3000 Bern 9, Switzerland.

*To whom correspondence should be addressed; E-mail: henrik.ronnow@epfl.ch

functions and, restricted by the local symmetry, gives the following crystal field Hamiltonian

$$\mathcal{H}_{CF} = \sum_{l=2,4,6} B_l^0 \mathbf{O}_l^0 + \sum_{l=4,6} B_l^4(c)\mathbf{O}_l^4(c) + B_6^4(s)\mathbf{O}_6^4(s) \quad (1)$$

$\mathbf{O}_l^m$ are the Stevens operators with amplitudes B_l^m [see (*9*) for definitions]. The dominant crystal field component is $\mathbf{O}_2^0 = 3J_z^2 - J(J+1)$, where the operator J_z is the component of the electronic angular momentum (J) along the z axis. In $LiHoF_4$, a negative B_2^0 leads to strong z axis Ising anisotropy, whereas a positive B_2^0 leads to planar XY anisotropy in $LiErF_4$.

The full magnetic Hamiltonian for Li*REF*$_4$ contains crystal field, external field (H), and hyperfine coupling to the nuclear spins, as well as dipolar and exchange interactions

$$\mathcal{H} = \sum_i [\mathcal{H}_{CF}(\mathbf{J}_i) - g_L \mu_B \mathbf{J}_i \cdot H + A\mathbf{J}_i \cdot \mathbf{I}_i] - \frac{1}{2}\sum_{ij}\sum_{\alpha\beta} \mathcal{J}_D D_{ij}^{\alpha\beta} J_{i\alpha} J_{j\beta} - \frac{1}{2}\sum_{ij,n.n.} \mathcal{J}_{ex}\mathbf{J}_i \cdot \mathbf{J}_j \quad (2)$$

where $\mathbf{J}_i$ and $\mathbf{I}_i$ are the electronic and nuclear angular momentum operators at site i. The electronic dipole moment is given by the angular momentum multiplied by the Bohr magneton μ_B and the Landé factor $g_L = 1.2$. The strength of hyperfine, exchange, and dipolar couplings are defined by A, $\mathcal{J}_{ex}$, and $\mathcal{J}_D$, respectively. The dipole interaction is the tensor

$$D_{ij}^{\alpha\beta} = \frac{3(r_{i\alpha} - r_{j\alpha})(r_{i\beta} - r_{j\beta}) - |\mathbf{r}_i - \mathbf{r}_j|^2 \delta_{\alpha\beta}}{|\mathbf{r}_i - \mathbf{r}_j|^5} \quad (3)$$

where $\mathbf{r}_i$ is the position of the ith ion. Its peculiar spatial anisotropy is illustrated in (Fig. 1). In $LiHoF_4$, the moments point along z, and nearest neighbors (NNs) are coupled ferromagnetically. In $LiErF_4$, in which the moments reside in the ab plane, half the NN couplings are AFM, the other half FM, and rotating the moments by 90° switches between FM and AFM interactions. In $LiHoF_4$, the exchange coupling is very small, on the order of 2% of the effective coupling at zero wave vector (*10*). Given the similar wave functions for Ho and Er, we also expect $\mathcal{J}_{ex}$ to be negligible in $LiErF_4$. The hyperfine coupling $A = 0.5(1)$ μeV for ^{167}Er (*11*) is weaker than $A = 3.36$ μeV in $LiHoF_4$ (*10*) and tunable because crystals can be prepared by using ^{168}Er without or ^{167}Er with nuclear moments. Our sample contained natural Er with 23% nuclear moments.

Limited data exist on the magnetic properties of $LiErF_4$. Electron paramagnetic resonance (EPR) (*12*, *13*), susceptibility, ^{7}Li nuclear magnetic resonance (NMR) (*14*), and optical spectroscopy (*15*) show planar XY anisotropy, but considerable variation in the reported anisotropy ratio and the lack of a globally consistent set of crystal field parameters prevented predictions of low-temperature properties. Susceptibility (*16*) and specific heat (*17*) show a transition around 380 mK. The shape of the specific heat anomaly differs from that of $LiHoF_4$ and 3D exchange-coupled XY materials, but the implied short-range correlations were discussed in terms of unlikely large exchange coupling. Susceptibility suggested AFM order (*18*), but the magnetic structure has not been determined. To this end, we have undertaken comprehensive neutron scattering, specific heat, and magnetic susceptibility studies.

The crystal field was determined by using neutron spectroscopy on a single crystal, providing not only the position of the energy levels but also the matrix elements of the angular momentum operators, more accurately defining the effective model (fig. S1). The ground state is a Kramers doublet isolated by a $\Delta = 2.25$ meV gap (tables S1 and S2). Within this subspace, an effective Hamiltonian for the low-temperature properties can be used in future theoretical work

$$\mathcal{H}_{\text{eff}} = \sum_{ij\alpha\beta} \mathcal{J}_{ij}^{\alpha\beta}\sigma_i^\alpha\sigma_j^\beta + g_\perp(\sigma_i^x B^x + \sigma_i^y B^y) + g_{||}\sigma_i^z B^z \quad (4)$$

where σ_i denotes the Pauli operators and $\mathcal{J}_{ij}^{\alpha\beta} = (\mu_B g_L)^2 C_\alpha C_\beta D_{ij}^{\alpha\beta}$, the magnetic coupling tensor between the effective $S = 1/2$ spins $S^\alpha = C_\alpha\sigma^\alpha$, with parameters calculated from the crystal field refinement: $C_x = C_y = 3.480$, $C_z = 0.940$, $g_\perp =$

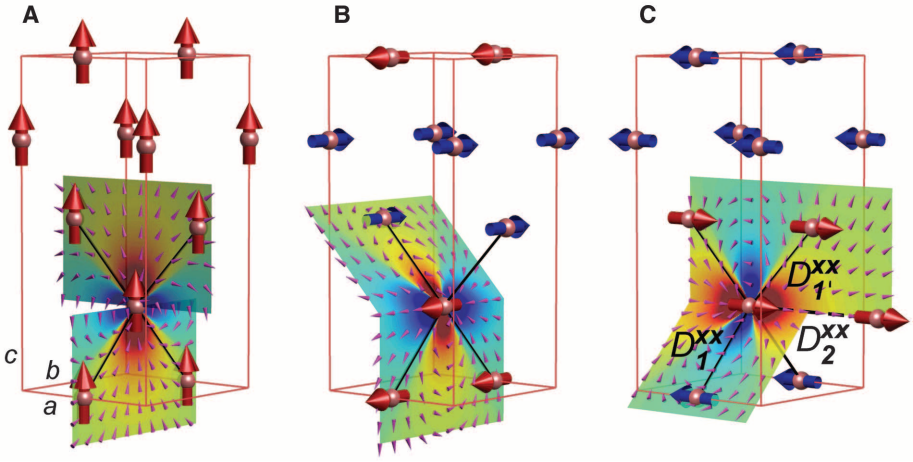

Fig. 1. Magnetic structures of Li*REF*$_4$. **(A)** Ferromagnetic c axis order in $LiHoF_4$, and BLAFM order with moments along **(B)** x or **(C)** y axis in $LiErF_4$. The dipole field from the central moment yields FM (red scale) and AFM (blue scale) coupling. Sign and strengths of the coupling depends on the direction of the moments. In the BLAFM structure, nearest and next-nearest couplings are $vD_1^{xx} = -5.5$ (AFM), $vD_{1'}^{xx} = 2.5$ (FM), and $vD_2^{xx} = 4.2$, $v = a^2c$. The crystal structure is tetragonal, space group $I4_1/a$ with $a = b = 5.162$ Å and $c = 10.70$ Å.

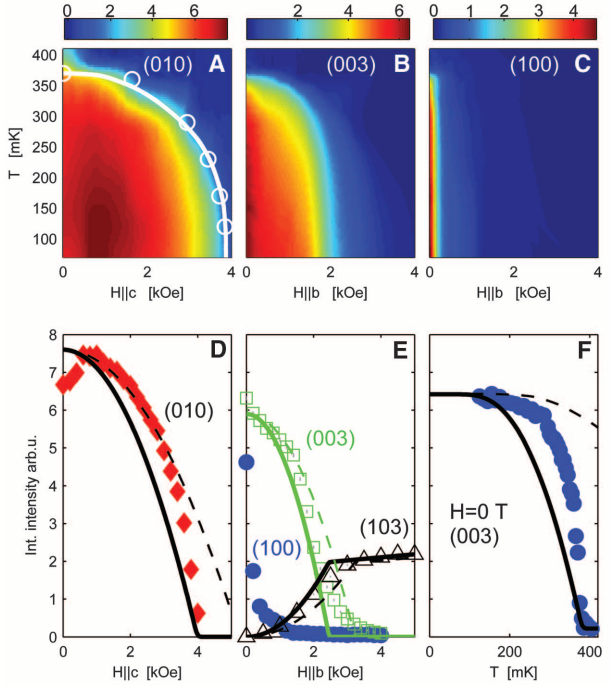

Fig. 2. (**A** to **C**) Field-temperature phase diagrams from the intensity of magnetic Bragg peaks: (010) with $H_{c||}$, (003) and (100) with $H_{b||}$, respectively. (**D** and **E**) Field dependence of peak intensities at $T = 100$ mK for field along c: (010) and along b: (100), (103), (003), respectively. (**F**) Temperature dependence of the (003) intensity. In (D) to (F), dashed lines are mean-field predictions, also shown in solid with temperature and field axes scaled by 0.52 and 0.76, respectively, to match the measured T_N and H_c.

$2g_L C_x = 8.35$, and $g_{||} = 2g_L C_z = 2.25$. Albeit the anisotropy ratio of the response to a magnetic field $g_\perp/g_{||} = 3.7$ is modest, the anisotropy ratio of the dipolar coupling $(g_\perp/g_{||})^2 = 13.8$ becomes large, which is what causes the XY anisotropy.

The magnetic structure was determined by means of single-crystal and powder neutron diffraction (fig. S2). Magnetic Bragg peaks at ($h + k + l$ = odd)—distinct from the structural peaks ($h + k + l$ = even)—prove explicitly AFM order. The single-crystal Bragg peak intensities are consistent with the bilayered antiferromagnetic (BLAFM) structure depicted in Fig. 1, and also verified by powder diffraction. The BLAFM has two equivalent configurations with moments along the a axis or b axis, respectively. A very small field of 300 Oe along the b axis suppresses the (100) reflection (Fig. 2E), populating a single a axis domain. Hence, the zero-field structure is a distribution of spatially separated domains with moments along a and b, respectively. Full powder refinement yielded an ordered moment $\langle J^x \rangle = 2.2 \pm 0.1$, reduced from the value $\langle J^x \rangle_{MF} = 3.0$ predicted by a MF calculation.

The phase diagram as function of temperature and fields along the c and b axes is shown in Fig. 2. The transition temperature $T_N = 373 \pm 5$ mK agrees with previous reports. For fields along c, the intensity at (010), corresponding to the order parameter squared, disappears in a sharp QPT at $H_{c||} = 4.0 \pm 0.1$ kOe. For fields along b, the (100) peak disappears owing to mono-domain formation. The (003) peak, which is independent of ab domains, decreases toward $H_{c\perp} \cong 2.1$ kOe, but a long tail remains to 4 kOe. The (103) peak, measuring the uniform FM component, grows toward a kink at $H_{c\perp}$, corresponding to maximal polarization of the ground-state doublet. Above $H_{c\perp}$, a weak linear increase, achieved by mixing-in higher lying crystal field levels, is well reproduced by the MF prediction.

A MF calculation yields the correct BLAFM ordered and a qualitatively correct phase diagram (supplementary materials). In $LiHoF_4$, a MF treatment accounts for most of the phase diagram except close to T_C, which is overestimated by 37% (*10*). In $LiErF_4$, $T_N^{mf} = 728$ mK, $H_{c||}^{mf} = 5.25$ kOe, and $H_{c\perp}^{mf} = 3.25$ kOe are all dramatically overestimated. Unlike $LiHoF_4$, any NN exchange interaction cancels in the BLAFM and cannot fine-tune the phase boundary. Including hyperfine coupling has little effect: $H_{c||} = 5.75$ kOe and $T_N = 735$ mK.

Scaling the temperature and field to match T_N and H_c, the $T_N(H)$ curve is well described (Fig. 2A), but the onset of order is more abrupt than the MF prediction (Fig. 2, D and E). Deep in the ordered phase, the unscaled MF calculation works (except for the low-field dip in Fig. 2D, which requires further investigation), but around the transition, fluctuations gain importance. We measured simultaneously the strength of the critical scattering, whose divergences independently determine T_N and H_c (Fig. 3, inset), increasing the precision of the extracted critical exponents: $\beta_T = 0.15 \pm$

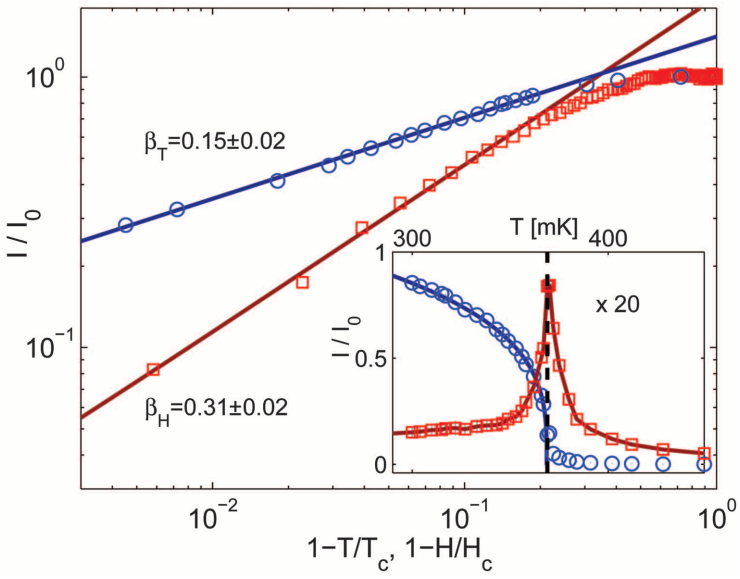

Fig. 3. (010) intensity as a function of temperature at $H = 0$ (blue circles) and a c axis field at $T = 80$ mK (red squares). Lines are power law fits. (Inset) Intensity of Bragg peak (blue circles) and critical scattering (red squares) extracted by fitting a resolution-corrected sum of a delta function and a Lorentzian to crystal rotation scans.

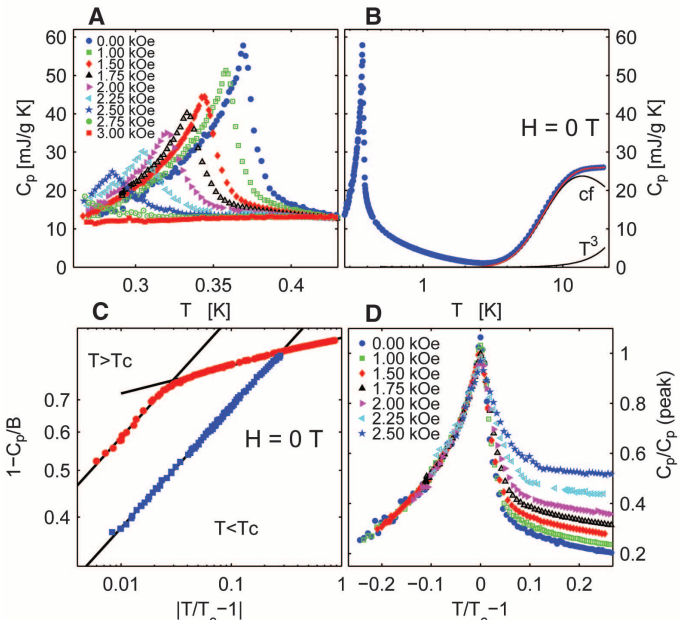

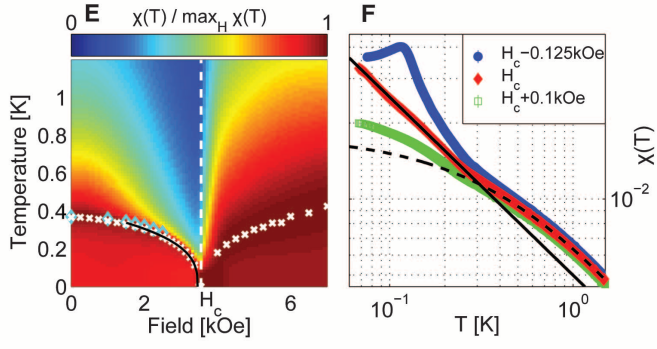

Fig. 4. (**A**) Specific heat versus temperature for several fields along the c axis. (**B**) Above 2K, specific heat is described by the sum (red line) of the crystal field Shottky anomaly (cf) and a very weak T^3 phonon contribution. (**C**) Power law behavior of specific heat at $H = 0$ T determines critical exponents. (**D**) Curves measured at different field values shifted to the same peak center and normalized by peak height to compare the evolution of peak shape. Below T_N, the data collapse onto a unique curve. (**E**) Susceptibility $\chi(T)$ normalized for each field. Peak positions are marked by crosses [$\chi(T)$] and diamonds [$C_p(T)$]. Black line is power law fit to $T_N(H)$. (**F**) $\chi(T)$ just below, at, and just above H_c. At H_c, $\chi(T)$ displays quantum critical scaling with exponent 0.70 ± 0.03 (solid line), up to a crossover around 250 mK, above which regular Curie-Weiss behavior $C/(T - \theta_{CW})$ with $\theta_{CW} = -0.55 \pm 0.01$ K describes the data (dashed line).

0.02 for the thermal transition at $H = 0$ T and $\beta_H = 0.31 \pm 0.02$ for the QPT at $H_{c\|}$ (Fig. 3). Both exponents considerably deviate from the MF expectation ($\beta^{mf} = [1/2]$).

The specific heat shows a pronounced ordering anomaly (Fig. 4), which is in good accordance with the phase diagram established by neutrons (figs. S3 and S4). The broad bump around 12 K is exactly described by our crystal field Hamiltonian. The phonon contribution ρT^3 with $\rho = (6.6 \pm 0.1) \times 10^{-7}$ J/gK^4 is much lower than previously reported for LiREF_4 (*17*), where the crystal field contribution was not subtracted. The tail above T_N is much more pronounced than in the FM cases of $LiHoF_4$ and $LiTbF_4$ (*17*, *19*, *20*). Around T_N, the specific heat follows a universal power law

$$C_p = A|t|^{-\alpha} + B \qquad t = T/T_c - 1 \qquad (5)$$

where $\alpha = -0.28 \pm 0.04$ below and above the transition, while $A_+/A_- = 1.68 \pm 0.04$ (A_+ and A_- are the values of the parameter A above and below the transition temperature, respectively). Subtracting B reveals a crossover to $\alpha = -0.07 \pm 0.05$ for $t > 0.03$ (Fig. 4C). Scaling to peak height and temperature, $C_p(T)$ curves for different fields collapse to a single unique curve below T_N (Fig. 4D).

For the classical phase transition, the exponent $\beta_T = 0.15 \pm 0.02$ is far from the $\beta = 0.3$ to 0.35 of standard 3D universality classes and instead falls in the window $\beta = 0.125$ to 0.23 for 2D XY criticality (*21*). Furthermore, the specific heat exponent $\alpha = -0.28 \pm 0.04$ is more negative than is the $\alpha = -0.13$ to -0.198 predicted for classical, dipolar, and quantum 3D Heisenberg models. Both exponents are consistent with recent Monte Carlo data on a dipolar 2D bilayer square lattice finding $\beta = 0.18 \pm 0.02$ and $\alpha \cong -0.4 \pm 0.2$ (*22*). Combining the Rushbrooke and Widom relations yields the exponent $\delta = (2-\alpha)/\beta - 1$, which describes the critical behavior of the (antiferromagnetic) order parameter versus (staggered) field $M \propto H^{1/\delta}$ at the transition. Together with $\eta = 2-d(\delta-1)/(\delta+1)$, δ is super-universal, depending only on the spatial dimension: $\delta = 4.7$, $\eta = 0.03$ for 3D (Ising, XY, and Heisenberg), and $\delta = 15$, $\eta = 0.25$ for 2D (Ising and XY/h_4). The exponent $\delta = 14.2$ for $LiErF_4$ is close to the 2D values. If the anomalous scaling dimension η of the spatial correlation function $\langle S_0 S_r \rangle \propto |r|^{d-2+\eta}$ at the critical point is zero, the critical properties can be derived with straightforward dimensional analysis—assuming 2D fluctuations in $LiErF_4$ yields $\eta = 0.26$, signaling strong fluctuations, which is consistent with the large reduction in transition temperature compared with the MF prediction.

The Mermin-Wagner theorem excludes long-range order in pure 2D XY models, but even infinitesimal fourfold (h_4) anisotropy leads to conventional order slightly above the Kosterlitz-Thouless transition. Weak h_4 anisotropy results in the effective exponents $\eta \cong 0.35$ and $\beta \cong 0.23$ (*21*), which on increasing h_4 approach $\eta = 0.25$ and $\beta = 0.125$—the Onsager solution for 2D Ising magnets. The Onsager solution also predicts a transition temperature reduced from the MF expectation by a factor of $T_c/T_c^{mf} = 1/2\log(1+\sqrt{2}) \cong 0.56$ for a NN square lattice model. This is close to our experimental value of $T_N/T_N^{mf} = 0.52$ in $LiErF_4$, but a theoretical effort is needed to generalize the Onsager solution to dipolar compounds.

It is surprising that we obtain 2D quasi-Ising-like exponents for a system whose two-dimensionality is not apparent from simple inspections of the direct and reciprocal crystal lattices and where the local symmetry was believed to be XY-like. For our data to be related to these models, two ingredients are needed: (i) reduction of spatial dimensionality from three to two and (ii) reduction of spin space dimensionality from one (XY) to zero (Ising). We leave the origins of these dimensional reductions as a topic for future theoretical efforts, noting here only that quantum fluctuations acting in concert with the tensorial nature of the dipolar interaction could give rise to (ii) through the phenomenon of order-by-disorder (*23*, *24*). Indeed, an estimate of the h_4 anisotropy due to order-by-disorder is of the correct order of magnitude to yield $\beta = 0.15$ (details available in the supplementary materials). The long history of theoretical studies of the 2D dipolar-coupled rotor model was recently revived through advances in microfabricated artificial nanomagnet arrays, which are pursued both as model systems for fundamental physics (*25*) and for ultrahigh-density magnetic storage technology (*26*, *27*). $LiErF_4$, which we see falls into this universality class, now provides a bulk material with a fully determined Hamiltonian with which theoretical predictions can be guided and tested.

Turning to the quantum phase transition, we observed an order parameter exponent $\beta_H = 0.31 \pm 0.02$ consistent with classical 3D scaling, thus confirming the long-standing Hertz result that a QPT in a d-dimensional system (2D XY/h_4 in our case) scales as a classical system in $d + 1$ dimensions (*28*). The detailed shape of the phase boundary was determined from susceptibility measurements (Fig. 4, E and F). Above 2 kOe, $T_N(H)$ scales as a power law with exponent 0.34 ± 0.01. At H_c, $\chi(T)$ exhibits quantum critical scaling, following a power-law exponent 0.70 ± 0.03 up to 250 mK, above which it crosses over to classical Curie-Weiss behavior. This behavior around the QCP is in stark contrast to the MF behavior observed in FM $LiHoF_4$. The exponent is close to the 0.75 reported for the heavy Fermion metal $CeCu_{6-x}Au_x$ near quantum criticality (*29*).

For $LiHo_xY_{1-x}F_4$, much recent theoretical interest focused on random fields, off-diagonal terms of the dipole interaction, and the emergence of glassiness (*30*–*32*). We expect $LiErF_4$ to show dramatic effects of dilution with nonmagnetic ions, or enhancement of off-diagonal terms via substitution of Ho for Er ions. An added benefit of Er is the existence of isotopes with and without nuclear spins, allowing comparative exploration of decoherence and mixing effects (*33*, *34*). Compared with other insulating or itinerant systems, $LiErF_4$ has the advantage of a simple, well-characterized Hamiltonian and of being available in large, high-quality single crystals; it promises insights into the fundamental science of quantum dipolar antiferromagnetism.

References and Notes

1. J. M. Luttinger, L. Tisza, *Phys. Rev.* **70**, 954 (1946).
2. J. Als-Nielsen, *Phys. Rev. Lett.* **37**, 1161 (1976).
3. R. Giraud, W. Wernsdorfer, A. M. Tkachuk, D. Mailly, B. Barbara, *Phys. Rev. Lett.* **87**, 057203 (2001).
4. W. Wu, B. Ellman, T. F. Rosenbaum, G. Aeppli, D. H. Reich, *Phys. Rev. Lett.* **67**, 2076 (1991).
5. P. E. Jönsson, R. Mathieu, W. Wernsdorfer, A. M. Tkachuk, B. Barbara, *Phys. Rev. Lett.* **98**, 256403 (2007).
6. J. A. Quilliam, S. Meng, C. G. A. Mugford, J. B. Kycia, *Phys. Rev. Lett.* **101**, 187204 (2008).
7. D. Bitko, T. F. Rosenbaum, G. Aeppli, *Phys. Rev. Lett.* **77**, 940 (1996).
8. D. H. Reich *et al.*, *Phys. Rev. B* **42**, 4631 (1990).
9. J. Jensen, A. R. Mackintosh, *Rare Earth Magnetism* (Clarendon, Oxford, 1991).
10. H. M. Rønnow *et al.*, *Phys. Rev. B* **75**, 054426 (2007).
11. J. P. Sattler, J. Nemarich, *Phys. Rev. B* **4**, 1 (1971).
12. M. R. Brown, K. G. Roots, W. A. Shand, *J. Phys. C Solid State Phys.* **2**, 593 (1969).
13. J. Magariño, J. Tuchendler, P. Beauvillain, I. Laursen, *Phys. Rev. B* **21**, 18 (1980).
14. P. E. Hansen, T. Johansson, R. Nevald, *Phys. Rev. B* **12**, 5315 (1975).
15. H. P. Christensen, *Phys. Rev. B* **19**, 6564 (1979).
16. P. Beauvillain, J. P. Renard, P. E. Hansen, *J. Phys. Chem.* **10**, L709 (1977).
17. G. Mennenga, L. J. de Jong, W. J. Huiskamp, *J. Magn. Magn. Mater.* **44**, 48 (1984).
18. K. S. Misra, J. Felsteiner, *Phys. Rev. B* **15**, 4309 (1977).
19. G. Ahlers, A. Kornblit, H. J. Guggenheim, *Phys. Rev. Lett.* **34**, 1227 (1975).
20. J. Nikkel, B. Ellman, *Phys. Rev. B* **64**, 214420 (2001).
21. A. Taroni, S. T. Bramwell, P. C. W. Holdsworth, *J. Phys. Condens. Matter* **20**, 275233 (2008).
22. L. A. S. Mól, B. V. Costa, *Phys. Rev. B* **79**, 054404 (2009).
23. J. Villain, R. Bidaux, J. P. Carton, R. Conte, *J. Phys. (Paris)* **41**, 1263 (1980).
24. C. L. Henley, *Phys. Rev. Lett.* **73**, 2788 (1994).
25. R. F. Wang *et al.*, *Nature* **439**, 303 (2006).
26. J. I. Martín, J. Nogués, K. Liu, J. L. Vicent, K. Ivan Schuller, *J. Magn. Magn. Mater.* **256**, 449 (2003).
27. M. V. Lubarda, S. Li, B. Livshitz, E. E. Fullerton, V. Lomakin, *Appl. Phys. Lett.* **98**, 012513 (2011).
28. A. J. Hertz, *Phys. Rev. B* **14**, 1165 (1976).
29. A. Schröder, G. Aeppli, E. Bucher, R. Ramazashvili, P. Coleman, *Phys. Rev. Lett.* **80**, 5623 (1998).
30. D. M. Silevitch *et al.*, *Nature* **448**, 567 (2007).
31. M. Schechter, N. Laflorencie, *Phys. Rev. Lett.* **97**, 137204 (2006).
32. S. M. A. Tabei, M. J. P. Gingras, Y. J. Kao, P. Stasiak, J. Y. Fortin, *Phys. Rev. Lett.* **97**, 237203 (2006).
33. N. V. Prokof'ev, P. C. E. Stamp, *Rep. Prog. Phys.* **63**, 669 (2000).
34. H. M. Rønnow *et al.*, *Science* **308**, 389 (2005).

Acknowledgments: We gratefully acknowledge fruitful discussions with J. Mesot, J. Jensen, A. J. Fisher, S. T. Bramwell, and S. Sachdev; support from Swiss National Science Foundation and Materials with Novel Electronic Properties; and neutron beam access at the Berlin Neutron Scattering Center, Helmholz-Zentrum Berlin, and the Swiss Spallation Neutron Source, Paul Scherrer Institut. Work at the University of Chicago was supported by the U.S. Department of Energy Basic Energy Sciences, the NSF Materials Research Science and Engineering Center, and the London Centre for Nanotechnology by the UK Engineering and Physical Sciences Research Council.

Supplementary Materials

www.sciencemag.org/cgi/content/full/336/6087/1416/DC1
Materials and Methods
Figs. S1 to S4
Tables S1 to S3

13 March 2012; accepted 19 April 2012
10.1126/science.1221878